Green Chemistry

Molten Plastics Induced Noncovalent Interactions for Tunable Cellulose Fast Pyrolysis

Journal:	*Green Chemistry*
Manuscript ID	GC-ART-04-2023-001312.R2
Article Type:	Paper
Date Submitted by the Author:	17-Oct-2023
Complete List of Authors:	Sakirler, Fuat; University of Massachusetts Lowell, Department of Chemical Engineering Tekbas, Mihriye; University of Massachusetts Lowell, Department of Chemical Engineering Wong, Hsi-Wu; University of Massachusetts Lowell, Department of Chemical Engineering

Molten Plastics Induced Noncovalent Interactions for Tunable Cellulose Fast Pyrolysis

Fuat Sakirler, Mihriye Doga Tekbas, and Hsi-Wu Wong*

Department of Chemical Engineering, University of Massachusetts Lowell

One University Avenue, Lowell, Massachusetts 01854, United States

Corresponding Author

*E-mail: hsiwu_wong@uml.edu

Abstract

Fast pyrolysis of lignocellulosic biomass is a promising approach for producing biofuels and renewable chemicals, but the resultant bio-oil quality and diverse product distributions limit its widespread adaptation. Concurrently, accumulation of waste plastics in the environment, particularly polyolefin thermoplastics, is becoming a growing threat. Co-pyrolysis of biomass with hydrogen-rich thermoplastics has shown promises for producing high-quality bio-oils, presenting an attractive solution to waste management. However, molecular-level understanding on the synergy of the two components in the melt phase during co-pyrolysis is still lacking. In this work, we report the discovery of catalytic and inhibitory effects on cellulose fast pyrolysis caused by noncovalent interactions (NCIs) induced by molten plastics. Our microreactor experiments demonstrated that selectivity toward cellulose-derived anhydrosugars, small oxygenates, or furans each increased due to the presence of polyketone, polyethylene glycol, or polystyrene, three thermoplastics with distinct functional groups. Density functional theory calculations reveal that key cellulose pyrolysis pathways leading to major products are catalyzed or inhibited due to perturbations of transition state geometries and partial charges caused by the NCIs induced by plastic functional groups. This discovery offers insights and opportunities for tuning cellulose fast pyrolysis via NCIs using a new family of unconventional molten plastic catalysts or inhibitors.

Introduction

Driven by increasing population, global energy demand is expected to grow more than 50% by 2050. Excessive usage of fossil-derived energy has resulted in diminishing fossil reserves and increasing environmental concerns. Lignocellulosic (inedible) biomass is an abundant and low-cost feedstock for producing renewable fuels and chemicals. Among the different biomass conversion methods, fast pyrolysis is a promising thermochemical route capable of producing high yields (up to 75 wt%) of liquid products called bio-oil as a potential renewable energy source.[1] Its economic viability, however, is hampered by the complexity of bio-oils typically composed of more than 300 molecules.[2, 3] The rich oxygen content of bio-oils also lowers fuel quality (e.g., calorific value, viscosity, water content, density, pH, etc.), making oxygen removal *via* chemical upgrading necessary.[4, 5]

Concurrently, accumulation of waste plastics in the environment is becoming a growing threat.[6, 7] Particularly, polyolefin thermoplastics, mainly polyethylene (PE), polypropylene (PP), and polystyrene (PS), consist of more than 71 wt% of plastic waste and are the least recycled.[8] Both waste biomass (such as yard trimmings and wood) and plastics are important components of municipal solid waste (MSW) in the United States, making up 18 and 12 wt%, respectively.[8] Co-processing of biomass with hydrogen-rich polyolefins presents an opportunity for simultaneous biofuel production and waste utilization, with the potential of also reducing the expensive sorting cost.[9] The same strategy can also be applied to treat waste biomass/plastic composites, such as plastic coated papers[10, 11] that are typically disposed of through landfills or incineration.

Co-pyrolysis of biomass and plastics has been shown to result in decreased bio-char yields and increased production of bio-oils of enhanced quality.[12-14] However, the synergy between the two components in this process is still debated. Since the degradation timescales of biomass (1–3 s at 500°C)[15] and common thermoplastics (from 2–5 min for PS to 25–45 min for PE at 500°C)[16, 17] are drastically different, several researchers hypothesized that no synergy between the two components could occur.[18-20] Indeed, most co-pyrolysis experiments observed only biomass-derived and plastics-derived products. Products from the coupling of the two components are generally found in low yields or non-existence unless a heterogenous catalyst is used.[21, 22] On the other hand, product yields from co-pyrolysis typically deviate from the arithmetic average of those from individual neat pyrolysis, suggesting underlying synergy possibly caused by the complex interplay between mass transfer and chemical kinetics driven by catalytic or inhibitory effects.

Several mechanisms have been proposed to account for the possible synergistic effects during biomass–plastics co-pyrolysis. Isotopic labeling studies suggest that radical coupling reactions would only occur in the presence of a heterogeneous catalyst, such as ZSM-5.[23] For co-pyrolysis involving cellulose (CE) without the presence of a catalyst, gas-phase interactions have been

explained by hydrogen atom transfer between the radicals derived from levoglucosan (LG) and plastics.[24, 25] This synergy is believed to suppress LG fragmentation in the gas phase and inhibit LG condensation and repolymerization, leading to increased LG yields. The evolution of biomass pyrolysis in the molten plastic phase, on the other hand, is less understood. It has been demonstrated that plastics physically inhibit the escape of CE-derived volatiles in the molten plastic phase,[24, 26] leading to higher yields of LG and low-molecular-weight products (LMWPs).[27, 28] The distributions of CE-derived products also markedly differ in the presence of plastics of different functional groups,[29] suggesting that the kinetics of CE pyrolysis is altered. However, the prospective of catalytic and inhibitory effects caused by the presence of molten plastic functional groups on CE pyrolysis, to our knowledge, is never discussed.

Recently, experiments conducted using the state-of-the-art pulsed heated analysis of solid reactions (PHASR) system by Dauenhauer and co-workers[30] have shed lights on the potential catalytic effect on CE fast pyrolysis caused by noncovalent interactions (NCIs). In their work, CE pyrolysis is accelerated by the presence of a nonvolatile compound (e.g., sorbitol or fructose) containing hydroxyl groups, suggesting NCI-induced catalytic effects in the molten phase.[30] Our recent density functional theory (DFT) study also suggests that intermolecular and intramolecular NCIs, such as hydrogen bonding, induce differences in Gibbs free energy *via* transition-state stabilization or destabilization, leading to catalytic or inhibitory effects on LG formation.[31] It can thus be hypothesized that functional groups in molten thermoplastics also perturb the reaction kinetics of CE fast pyrolysis by inducing NCIs during CE–plastics co-pyrolysis. If such NCI-induced catalytic or inhibitory effects are thoroughly understood and harnessed, synergistic interactions during CE–plastics co-pyrolysis could be manipulated to selectively promote certain reaction pathways leading to desired value-added products. This will significantly improve the economic viability and outlook of the pyrolysis technologies for treating heterogeneous waste streams containing mixtures of biomass and plastics.

To elucidate the molecular-level understanding of how molten plastic functional groups affect the kinetics of biomass pyrolysis during biomass–plastics co-pyrolysis, co-pyrolysis of CE with PE, PS, polyethylene glycol (PEG), or polyketone (PK) were studied using both microreactor experiments and DFT calculations. CE was selected as a model biomass due to its simple structure and rich amount of knowledge and literature data about its pyrolysis chemistry. Each of the plastics was chosen to contain none (PE) or only one type of functional groups (aromatic, ether, or ketone groups in PS, PEG, or PK, respectively) for unbiased comparisons. Each of the selected biomass and plastic model components has a distinct product distribution from its neat pyrolysis. By conducting model compound studies, the complexity of analyzing the products and their origins in co-pyrolysis is significantly reduced. Experiments were conducted in a custom-made microreactor under vacuum to suppress secondary gas-phase reactions for better examination of interactions occurring in the molten phase. DFT calculations were performed to study

the formation pathways of key CE-derived products using cellobiose as a model compound, where the DFT-calculated rate parameters of the major reactions leading to LG, glycolaldehyde (GA), and 5-hydroxymethylfurfural (5-HMF) in the presence of surrogate functional groups were compared against the experimentally determined selectivity toward these species. Our work uncovers how functional groups in molten plastics mediate acceleration (catalytic) or deceleration (inhibitory) of CE fast pyrolysis *via* NCIs during CE–plastics co-pyrolysis.

Results and Discussion

Co-pyrolysis of Cellulose and Plastics

Figure 1a shows the mass yields of CE-derived products from neat CE pyrolysis as well as binary co-pyrolysis of CE with PE, PS, PEG, or PK at 500°C under vacuum. Numerical values of the mass yields and their uncertainties are also provided in **Table S1** of Supporting Information (SI). The corresponding carbon yields are shown in **Figure S1a** and provided in **Table S2** of SI. Major products from neat CE pyrolysis include anhydrosugars (e.g., LG), small oxygenated (e.g., GA), and furans (e.g., 5-HMF). They are distinct from those from neat pyrolysis of PE (which mainly produces linear aliphatic hydrocarbons, as listed in **Table S3** of SI), PS (which mainly produces benzene, toluene, styrene, styrene dimer, and styrene trimer, as listed in **Table S4** of SI), and PEG (which mainly produces linear glycol ethers, as listed in **Table S5** of SI). No products were observed from neat PK pyrolysis due to its thermal stability under this reaction condition.

Interestingly, no new major products were observed in all co-pyrolysis experiments. Instead, product distributions resemble neat pyrolysis of individual components, yet yields of the products were significantly shifted. This can be explained by the study by Dorado *et al.*,[23] which shows that new products from the coupling co-pyrolysis reactions were only observed when a heterogeneous catalyst was used, in such case isotopic labeling was needed to determine product origins. Given the fact that no coupling products were observed in our co-pyrolysis experiments, the origins of the products from co-pyrolysis can be attributed to the individual components.

The mass balance for CE-derived products did not close in this study since CE-derived anhydrosugar oligomers (e.g., cellobiosan, cellotriosan, cellotetrasan, etc.) and water vapor were not detected by gas chromatography. However, our neat CE thin-film pyrolysis, with an estimated initial heating rate of 2,300 ^{o}C s^{-1} (see Section S4 of the SI), resulted in a 14.3 wt% LG yield, comparable with the 10–15 wt% LG yields from the PHASR experiments.[30]

The presence of plastics led to enhanced combined yields of cellulose-derived volatiles (products other than gases and char) to the range of 15.5–35.6 wt%, mainly contributed by increased LG yields by 13.9–34.3 wt%. Mass yields of LMWPs, particularly

small oxygenates and furans, also increased by 1.3–9.3 wt%. As suggested in our previous work,[28] the evaporation of anhydrosugar oligomers and the thermal ejection of aerosols are inhibited by the molten plastic phase, promoting further decomposition of anhydrosugar oligomers and aerosols into LG and LMWPs. This was also evidenced by the reduced undetected mass in the presence of plastics.

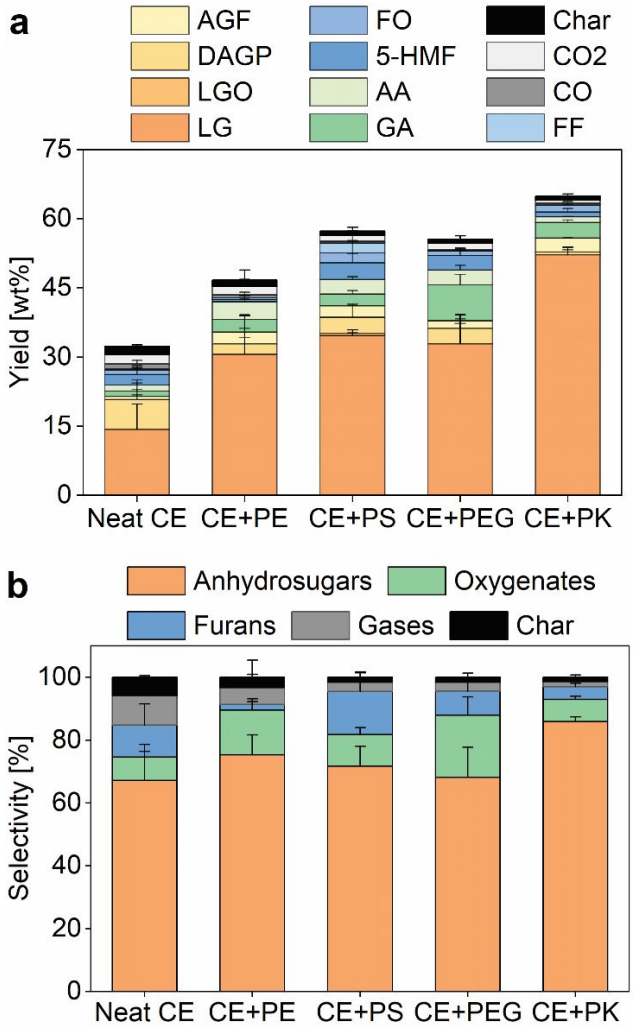

Figure 1. (a) Mass yields of CE-derived products and (b) selectivity toward CE-derived anhydrosugars, small oxygenates, furans, gases, and char from neat CE pyrolysis and co-pyrolysis of CE with PE (CE+PE), PS (CE+PS), PEG (CE+PEG), or PK (CE+PK). Yields are shown for levoglucosan (LG), levoglucosenone (LGO), dianhydroglucopyranose (DAGP), 1,6-anhydroglucofuranose (AGF), glycolaldehyde (GA), acetic acid (AA), 5-hydroxymethylfurfural (5-HMF), 2-(5H)-furanone (FO), furfural (FF), carbon monoxide (CO), carbon dioxide (CO_2), and char. Reaction condition: 5.0 mg of CE co-pyrolyzed with PE (3.08 mg), PS (4.10 mg), PEG (3.48 mg), or PK (4.03 mg) at 500°C under vacuum (< 0.04 torr). The mass loading of each plastic component was chosen to ensure that the thickness of the samples was kept constant and the extent of inhibition of evaporation and thermal ejection approximately equal.

While the increased yields of CE-derived products were universal in the presence of all four plastics, the differences in product distributions reflect additional underlying effects.[29] Since no new CE-derived products were observed, the different product distributions could be emanated from the acceleration (being catalyzed) or deceleration (being inhibited) of the CE pyrolysis pathways. These catalytic and inhibitory effects are likely caused by the different plastic functional groups, where concert actions of multiple NCIs, such as hydrogen bonding, van der Waals forces, and electrostatic interactions, take effect. Note that the thickness of the binary CE–plastics samples was held constant in our co-pyrolysis experiments to keep the extent of inhibition of evaporation and thermal ejection approximately equal. Co-pyrolysis experiments of CE with PS, PEG, or PK (denoted as CE+PS, CE+PEG, or CE+PK, respectively) are compared against those with PE (denoted as CE+PE). This is done because PE does not contain any functional groups, allowing the determination of unbiased catalytic or inhibitory effects caused by the plastic functional groups.

We further grouped CE-derived products into three families of bio-oil compounds: i) anhydrosugars, ii) small oxygenates, and iii) furans, along with iv) gases, and v) char. Our experiments showed that the selectivity toward anhydrosugars significantly increased in the presence of PK, by 10.6 % compared to that in the presence of PE (**Figure 1b** and **Figure S1b** of SI), while the presence of PS or PEG led to decreased anhydrosugar selectivity by 3.6 or 7.2 %. The selectivity toward small oxygenates increased by 5.7 % in the presence of PEG compared to that in the presence of PE, whereas the selectivity toward small oxygenates decreased by 4.1 or 7.1 % in the presence of PS or PK. Finally, the selectivity toward furans all increased regardless of the plastic type, with the presence of PS leading to the most enhancement by 11.9 %, followed by the presence of PEG and PK.

Char formation in CE fast pyrolysis can be attributed to both primary and secondary reactions.[2, 32] Using thin-film samples under vacuum could limit secondary gas-phase dehydration leading to char and thus inhibits its formation.[32, 33] Indeed, the char yield from our neat CE pyrolysis was 1.9 wt% (**Figure 1a**), lower than the typical range of 5–8 wt% at atmospheric pressure,[33] agreeable with the 1–3 wt% from CE fast pyrolysis under vacuum using a fast-heating wire-mesh reactor (with an initial heating rate of ~5,000°C s^{-1}).[34] The presence of plastics in co-pyrolysis led to further reduction of char yields by up to 1 wt% compared to neat CE pyrolysis, agreeable with lower char yields observed from other biomass–plastics co-pyrolysis studies.[35] Note that char formation in our co-pyrolysis experiments can only or mostly be attributed to CE pyrolysis since no char was observed during individual neat pyrolysis of PE, PS, or PK, except for PEG where char yield was very low at 0.58 wt%. It is suggested by Mettler *et al*.[2] that gas-phase repolymerization or aldol condensation of volatile products may be the primary pathway for char formation in CE fast pyrolysis. Accordingly, the reduced char formation observed in our co-pyrolysis experiments could be explained by the dilution of volatiles in the presence of molten polymers, which inhibits bimolecular reactions leading to char. It

is also possible that in the presence of molten polymers, cellulose is dispersed in the molten polymer phase prior to the onset of pyrolysis, as suggested by Kumagai *et al.*,[35] suppressing repolymerization to achieve reduced char formation.

In our neat CE pyrolysis experiments, CO and CO_2 were the only gaseous products detected, at 1 and 2 wt%, respectively, consistent with literature values.[33, 34] The formation of CO and CO_2 is attributed only to CE since neither molecule was observed during neat pyrolysis of PE, PS, PEG, or PK. The presence of plastics all led to decreased CO and CO_2 yields, with the most significant effect caused by PK (**Figure 1a**). The decreased formation of CO and CO_2 is correlated with the reduced char yields in our co-pyrolysis experiments, since all three are the results of consecutive CE dehydration during pyrolysis.[15]

Effect of Functional Groups on the Formation of LG, GA, and 5-HMF

DFT calculations were performed to further explore the underlying molecular-level catalytic and inhibitory effects caused by the NCIs induced by molten plastics. The formation pathways leading to the most prominent product of each bio-oil product family, i.e., LG from anhydrosugars, GA from small oxygenates, and 5-HMF from furans, shown in **Scheme 1**,[31, 36-38] were selected for further analysis.

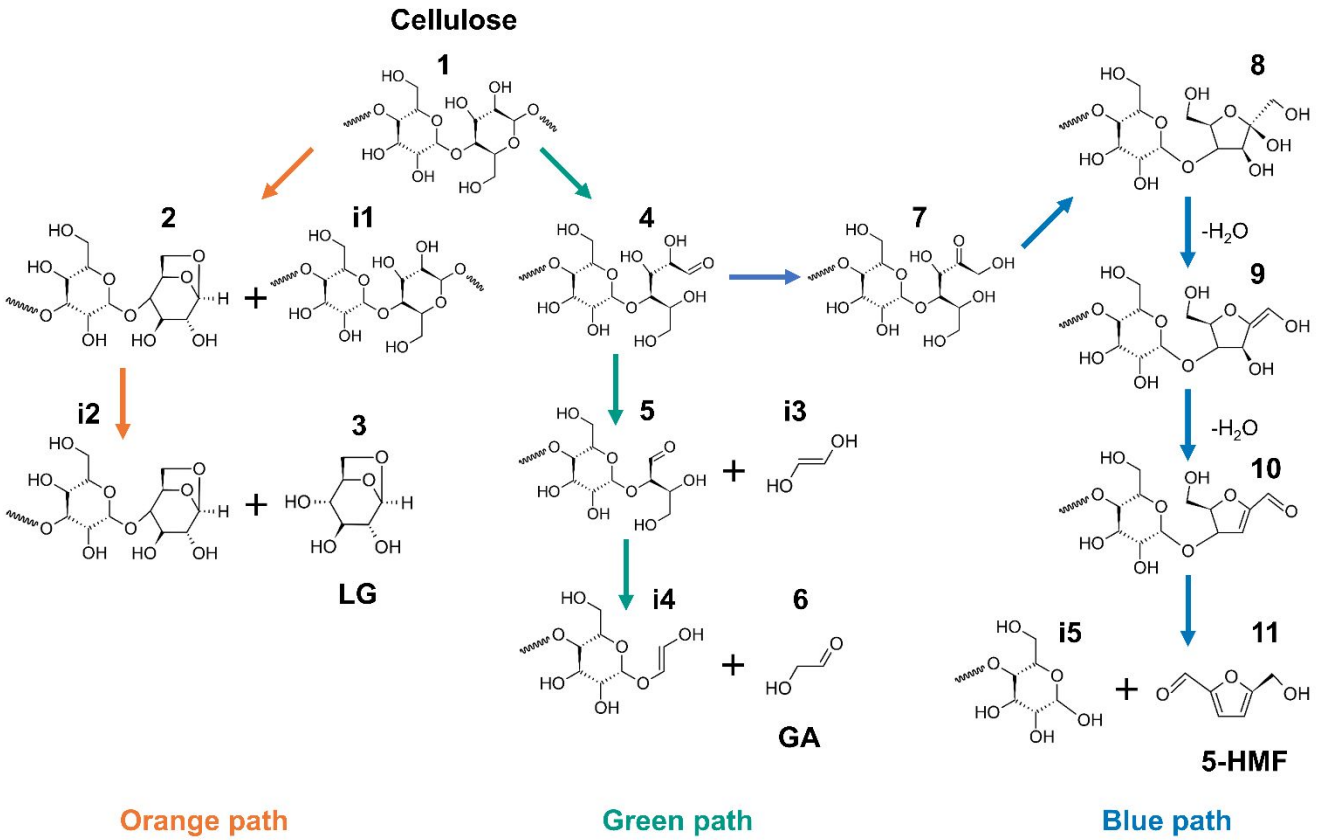

Scheme 1. Elementary steps of cellulose pyrolysis leading to levoglucosan (LG, **3**), glycolaldehyde (GA, **6**), and 5-hydroxymethylfurfural (5-HMF, **11**) investigated by DFT.

It is agreed that LG (**3**) is produced *via* β-1,4 glycosidic bond cleavage of the LG-like (reducing) end of an active CE chain[39] ("orange path" in **Scheme 1**). While several competing GA and 5-HMF formation pathways are suggested, experimental[40] and theoretical[37] findings agree that an acyclic glucose structure (**4**) originated from ring opening of the reducing end of active CE is the main precursor.[38] Note that ring opening of glucose is also hypothesized as a possible pathway leading to small oxygenates (e.g., GA)[41] and furans (e.g., 5-HMF).[36] However, little glucose is observed experimentally due to its evanescent nature,[42] and the hypothesized thermohydrolysis pathway for glucose formation is also unlikely due to the highly-packed CE crystalline structure that inhibits water contact with its interior units.[15] Furthermore, water readily evaporates under fast pyrolysis conditions (500°C), particularly at vacuum. Consequently, formation of small oxygenates and furans *via* glucose is not considered in this study.

Each elementary step in **Scheme 1** was first investigated by DFT using cellobiose (CB) as a model CE compound without any external molecules. The elementary steps for LG (orange path), GA (green path), and 5-HMF (blue path) formation were subsequently studied in the presence of propane (C3), benzene (Bz), dimethyl ether (DME), or acetone (Ace) as surrogates for PE, PS, PEG, or PK, respectively. The lowest Gibbs-free-energy conformations of the reactants and transition states (TSs) at 500°C were used to calculate kinetic parameters (**Tables S6** and **S7** of SI).

To allow comparison between experimental and DFT findings, a rate constant ratio (R) was used for each elementary step as a qualitative predictor of the DFT-calculated NCI strength (**Table S7** of SI). R is defined as the ratio of the rate constant in the presence of Bz, DME, or Ace (representing co-pyrolysis of CE with PS, PEG, or PK) to that in the presence of C3 (representing co-pyrolysis of CE with PE) as:

$$R(i,T) = k_x(i,T)/k_{C3}(i,T) \quad \text{x} = \text{Bz, DME, Ace} \tag{1}$$

where T is the reaction temperature. By examining the R value of each elementary step, catalytic (i.e., R>1) or inhibitory (i.e., R<1) effects caused by the presence of Bz, DME, or Ace can be easily identified. To verify the assumption that PE does not affect CE pyrolysis kinetics, rate parameters in the presence of C3 are also compared to those in the absence of any surrogates (k_{C3}/k_{neat} in **Table S6** of SI). Our DFT calculations suggest an average k_{C3}/k_{neat} value of 1.01 at 500°C, with a standard deviation of 0.14. This confirms that molten PE has negligible catalytic or inhibitory effects on CE pyrolysis.

LG Formation

LG formation is studied by DFT *via* glycosidic bond cleavage of CB (**1**) followed by a second glycosidic bond cleavage of cellobiosan (**2**) (**Scheme 1**). C−O cleavage in carbohydrate pyrolysis can proceed with either boat or the more favorable inverted-

chair conformation.[31, 41, 43] Low-energy conformations of C−O cleavage using CB for **1** → **2** + **i1** and cellobiosan for **2** → **3** + **i2** were studied. The first C−O cleavage (**1** → **2** + **i1**) leading to "active CE" was predicted to have an activation energy of 48.3 kcal mol^{-1}, 3.8 kcal mol^{-1} lower than that of the subsequent C−O cleavage (**2** → **3** + **i2**) leading to LG, suggesting that the second C−O cleavage reaction is the rate-limiting step in the absence of any surrogates (**Table S6** of SI).

The DFT-calculated *R* values for the elementary steps leading to LG formation (**1** → **2** + **i1** and **2** → **3** + **i2**) in the presence of C3, Bz, DME, or Ace (**Figure 2a**) suggest that each of the three functional groups inhibits the first C−O cleavage reaction (**1** → **2** + **i1**), with ether or ketone groups induce larger effect than aromatics. On the other hand, aromatic or ether groups induce an inhibitory effect on the second C−O cleavage reaction (**2** → **3** + **i2**, R_{Bz}=0.35 and R_{DME}=0.65), whereas ketone groups induce a catalytic effect (R_{Ace}=2.52). The increased experimental LG selectivity by 15.6 % in the presence of PK is agreeable with the DFT-predicted catalytic effect on LG formation **2** → **3** + **i2** caused by the presence of Ace (R_{Ace}=2.52), as shown in **Figure 2b**. Likewise, the decreased experimental LG selectivity by 4.4 or 5.7 % in the presence of PS or PEG, compared to that in the presence of PE (64.8 %), is agreeable with the DFT-predicted inhibitory effect on LG formation caused by the presence of Bz or DME (R_{Bz}=0.35 and R_{DME}=0.65). In general, our DFT results agree with the trends observed in our co-pyrolysis experiments.

Our previous DFT study has shown that hydroxyl groups near the reaction center can stabilize or destabilize C−O cleavage *via* hydrogen bonding with charge-separated TSs.[31] Here, the catalytic effect on the second C−O cleavage reaction caused by ketone groups (**2** → **3** + **i2**, R_{Ace}=2.52) is evidenced by a new intermolecular hydrogen bond (O2'−H···O_{Ace}, 2.33 Å) between the carbonyl oxygen atom of Ace and the O2' hydroxyl group of **2** (**Figure 2c**), lowering the activation energy of $\mathbf{TS2_{Ace}}$. The presence of Ace also causes perturbations of bond lengths and partial charges. Particularly, the intramolecular O2'−H···O1 hydrogen bond and the distance between O6 and H6 of $\mathbf{TS2_{Ace}}$ are shortened by 0.25 and 0.04 Å compared to $\mathbf{TS2_{C3}}$, respectively, indicating increased hydrogen bond strengths and TS stability. The stronger hydrogen bonds are also reflected by more negative charges on O6 and O1 of $\mathbf{TS2_{Ace}}$ than those of $\mathbf{TS2_{C3}}$ by 0.17 and 0.15 au, respectively, and more positive charges on H6 of $\mathbf{TS2_{Ace}}$ than that of $\mathbf{TS2_{C3}}$ by 0.14 au.

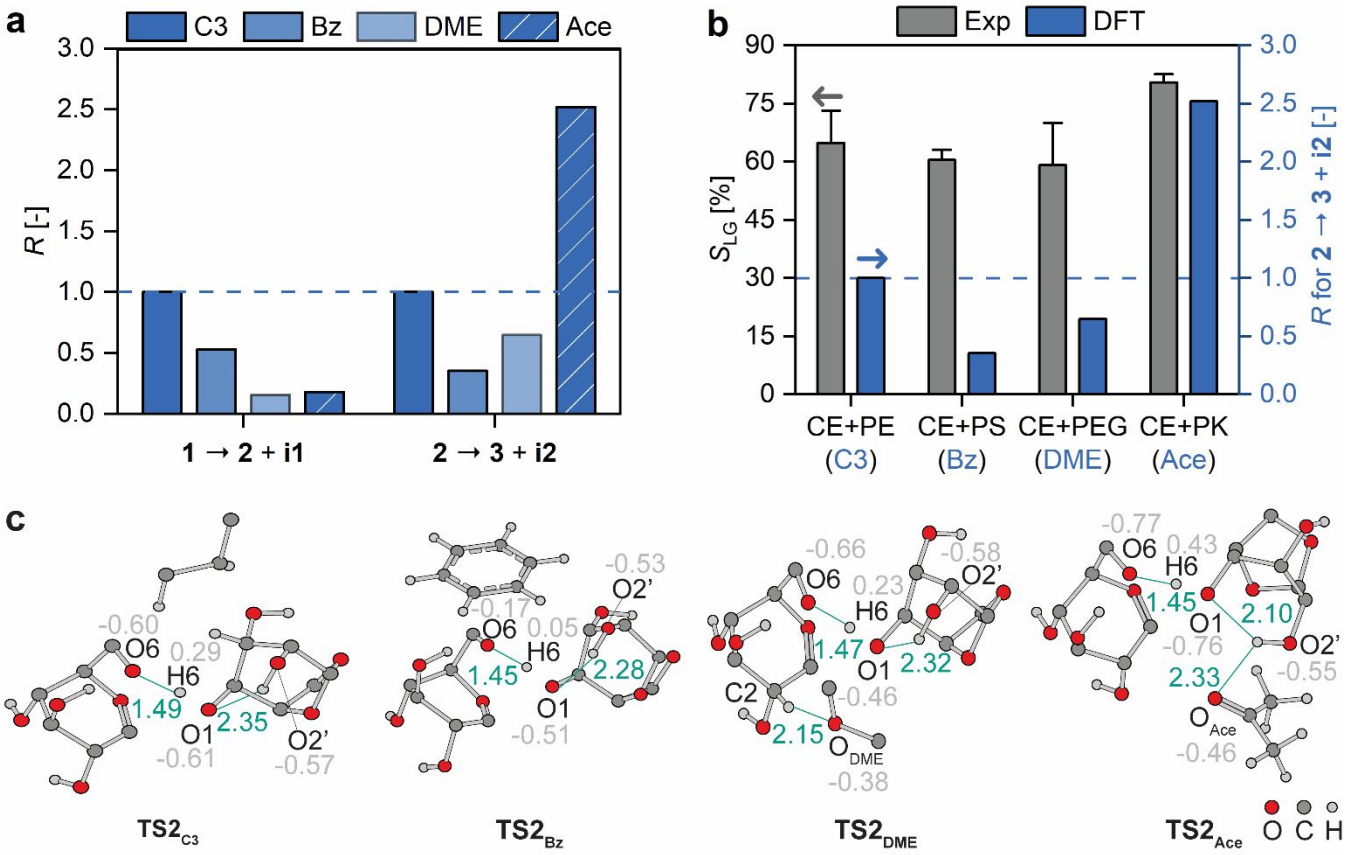

Figure 2. (a) DFT-calculated rate constant ratios (*R*) of the elementary steps leading to levoglucosan (LG) formation in the presence of C3, Bz, DME, or Ace at 500°C. (b) Comparison of selectivity toward LG from the co-pyrolysis experiments of CE with PE (CE+PE), PS (CE+PS), PEG (CE+PEG), or PK (CE+PK) against the *R* values for **2** → **3** + **i2** in the presence of plastic surrogates. (c) TSs for **2** → **3** + **i2** in the presence of C3, Bz, DME, or Ace including key distances and partial charges. Numbers in green and grey represent distances in Å and ChelpG partial charges in au, respectively. Hydrogen atoms not involved in noticeable interactions are omitted for clarity.

In contrast to the catalytic effect caused by ketone groups, aromatic or ether groups lead to an inhibitory effect on C−O cleavage **2** → **3** + **i2**. Compared to $\mathbf{TS2_{C3}}$, $\mathbf{TS2_{Bz}}$ has 0.43 and 0.10 au less negative charges on O6 and O1 (partial charges of -0.17 and -0.51 au, respectively) and a 0.24 au less positive partial charge on H6 (partial charge of 0.05 au), making $\mathbf{TS2_{Bz}}$ less susceptible to nucleophilic attack than $\mathbf{TS2_{C3}}$ (**2** → **3**, R_{Bz}=0.35).

In evaluating inhibited C−O cleavage in the presence of DME, negligible perturbations in O6−H6 distance and O2'−H···O1 hydrogen bond length was observed. The negative charge on O6 is increased by 0.06 au compared to $\mathbf{TS2_{C3}}$. Like ketone groups, ether groups also lead to an intermolecular hydrogen bond between C2 and O_{DME} (i.e., C2−H···O_{DME}, 2.15 Å). Given these observations, it would be reasonable to expect catalytic effects induced by ether groups. However, the negative charge on O_{DME}

is reduced by 0.08 au in **TS2$_{DME}$**, indicating a weaker hydrogen bond. In line with concerted action of stabilizing and destabilizing NCIs,[44] NCIs induced by ether groups result in an inhibitory effect on C−O cleavage **2** → **3** + **i2**.

GA Formation

GA (**6**) formation (green path) involves ring opening of CB (**1**) to **4**, followed by two consecutive retro-aldol reactions *via* **5** to GA (**Scheme 1**). Ring opening in glucose pyrolysis is believed to proceed with the chair, boat, and inverted-chair conformations,[41, 45] with inverted-chair the most favorable to produce acyclic glucose due to a stable six-atom cyclic TS. Lu *et al*. reported that ring opening from the reducing end of CB is approximately 29 kcal mol^{-1} more favorable than that from the non-reducing end.[37] Consequently, we only focused on ring opening of CB from the reducing end. We also discovered that the six-atom cyclic TS from the inverted-chair conformation was more stable by 3.5 kcal mol^{-1} than the four-atom cyclic TS from the chair conformation studied by Lu *et al*.[37] It is agreed that retro-aldol condensation is more favorable than ring opening in carbohydrate pyrolysis due to its low energy barrier.[37, 41] Our DFT calculations also corroborate that the rate constants of the consecutive retro-aldol condensation reactions of the acyclic glucose unit of intermediate **4** are four orders of magnitude higher than that of ring opening **1** → **4** in the absence of any surrogates. The activation energy of the ring opening reaction was calculated to be 48.0 kcal mol^{-1}, 11.7 and 15.1 kcal mol^{-1} higher than those of the two retro-aldol condensation reactions, suggesting that it is the rate-limiting step in GA formation (**Table S6** of SI).

The DFT-calculated *R* values for the elementary steps leading to GA formation in the presence of C3, Bz, DME, or Ace (**Figure 3a**) suggest that aromatic or ketone groups lead to an inhibitory effect on ring opening **1** → **4** (R_{Bz}=0.37, R_{Ace}=0.38), whereas ether groups result in a catalytic effect (R_{DME}=3.11). The first retro-aldol condensation **4** → **5** + **i3** is catalyzed by all three functional groups, with the most significant effect caused by aromatic groups (R_{Bz}=97.7). The second retro-aldol condensation **5** → **6** + **i4** is catalyzed only by aromatic groups (R_{Bz}=2.63), whereas ether and ketone groups lead to an inhibitory effect (R_{DME}=0.19, R_{Ace}=0.78). Our results also corroborate the reported effect of metal ions on glucose pyrolysis, which depends on the stereochemistry near the reaction center.[42]

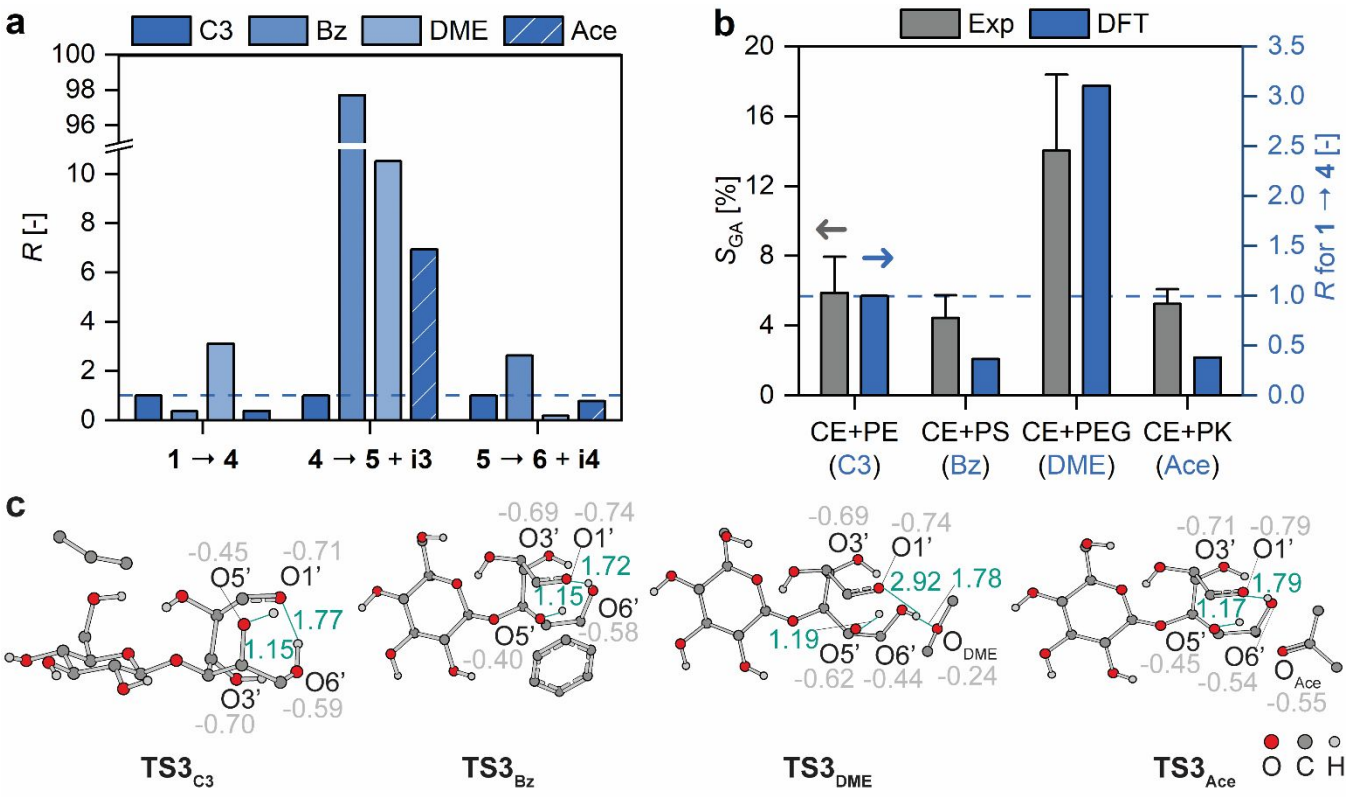

Figure 3. (a) DFT-calculated rate constant ratios (*R*) of the elementary steps leading to glycolaldehyde (GA) formation in the presence of C3, Bz, DME, or Ace at 500°C. (b) Comparison of selectivity toward GA from the co-pyrolysis experiments of CE with PE (CE+PE), PS (CE+PS), PEG (CE+PEG), or PK (CE+PK) against the *R* values for the rate-limiting step **1** → **4** in the presence of corresponding surrogates. (c) TSs for **1** → **4** in the presence of C3, Bz, DME, or Ace including key distances and partial charges. Numbers in green and grey represent distances in Å and ChelpG partial charges in au, respectively. Hydrogen atoms not involved in noticeable interactions are omitted for clarity.

Comparing the DFT-calculated *R* values against the selectivity toward GA from the co-pyrolysis experiments (**Figure 3b**) reveals that the increased experimental GA selectivity by 8.15 % in the presence of PEG compared to that in the presence of PE is consistent with the DFT-predicted catalytic effect on ring opening **1** → **4** caused by the presence of DME (R_{DME}=3.11). Likewise, the decreased experimental GA selectivity in the presence of PS or PK is consistent with the DFT-predicted inhibitory effect on ring opening **1** → **4** caused by the presence of Bz or Ace (R_{Bz}=0.37, R_{Ace}=0.38).

The DFT-calculated TSs for ring opening **1** → **4** further reveal that while the presence of Bz or Ace does not lead to significant perturbation in partial charges on O5' (**Figure 3c**), the presence of DME leads to 0.17 au more negative partial charge on O5' (a partial charge of -0.62 au), making **TS3$_{DME}$** more susceptible to proton transfer than **TS3$_{C3}$**. In addition, **TS3$_{DME}$** is stabilized by a new intermolecular hydrogen bond O6'−H···O_{DME}, breaking the intramolecular hydrogen bond O6'−H···O1'.

5-HMF Formation

It is suggested that 5-HMF formation *via* a fructose intermediate is the most favorable.[36, 46] Our work considers the following elementary steps leading to 5-HMF *via* a fructose-end intermediate ("blue path" in **Scheme 1**): ring opening from CB (**1**) to **4**, isomerization from **4** to **7** with an acyclic fructose end, ring closing from **7** to **8**, dehydration of **8** to **9**, a second dehydration of **9** to **10**, and finally C−O cleavage of **10** to 5-HMF (**11**). Our DFT calculations of CB pyrolysis corroborate the previous DFT studies,[37, 38] where dehydration **8** → **9** + H_2O has the highest energy barrier of 70.1 kcal mol^{-1}, making it the rate-limiting step (**Table S6** of SI).

The DFT-calculated *R* values for the elementary steps leading to 5-HMF in the presence of C3, Bz, DME, or Ace (**Figure 4a**) suggest that aromatic or ketone groups catalyze all elementary steps except ring opening **1** → **4**, yet their effects on each step vary. Specifically, aromatic groups significantly catalyze C−O cleavage (**10** → **11** + **i5**, R_{Bz}=11.1), while their effect on isomerization **4** → **7** (R_{Bz}=1.10) is negligible. The extent of catalytic effect caused by ketone groups on C−O cleavage is less pronounced (R_{Ace}=1.41), yet the first dehydration reaction (**8** → **9** + H_2O, R_{Ace}=15.2) is significantly catalyzed. On the other hand, ether groups catalyze all elementary steps except isomerization **4** → **7** (R_{DME}=0.31), with the most marked catalytic effect on ring closing **7** → **8** (R_{DME}=19.9).

It is shown in our co-pyrolysis experiments that the presence of PS, PEG, or PK all helped increase the selectivity toward 5-HMF compared to the presence of PE. This is consistent with the DFT-predicted catalytic effect on dehydration **8** → **9** + H_2O caused by the presence of the surrogates of thermoplastics with functional groups (**Figure 4b**). However, the extent of this catalytic effect has reverse trends. Specifically, experiments demonstrated that PS led to the highest increase in 5-HMF selectivity followed by PEG and PK, but DFT predicted that ketone groups have the largest catalytic effects followed by ether and aromatic groups. This reverse trend could be explained by the competing and coupling reaction pathways leading to CE-derived products which cannot be individually separated in the experiments.[47] It has been shown that increased LG formation leads to decreased LMWP yields in neat CE fast pyrolysis.[48] In our work, the presence of PK is predicted by DFT to favor the formation of both LG (**Figure 2b**) and 5-HMF (**Figure 4b**). Since their formation pathways are competing, the predicted catalytic effects could be negated. Indeed, the enhancement in both LG and 5-HMF yields in the experiments are less marked than the DFT-predicted *R* values. On the other hand, the presence of PS and PEG is predicted by DFT to suppressed LG formation (**Figure 2b**), which could in turn further facilitate the formation of 5-HMF. This explains that the marked changes in the experimental 5-HMF yields in the presence of PS and PEG compared to the DFT-predicted *R* values. Another possible explanation for this reversal is the multistep nature of 5-HMF formation, where the effect of the non-rate-limiting steps could be present.[49-51] For instance, C−O cleavage (**10**

→ **11** + **i5**), the second-slowest step at 500°C, may exert a comparable controlling effect on 5-HMF selectivity, where the extent of the catalytic effect predicted by DFT (R_{Bz}>R_{DME}>R_{Ace}) follows the same trend of the experimental 5-HMF selectivity. Rigorous and quantitative comparison between the DFT-calculated rate parameters and experimental yields would require full execution of a microkinetic model including all elementary reactions and is not the focus of this work.[42, 47, 52]

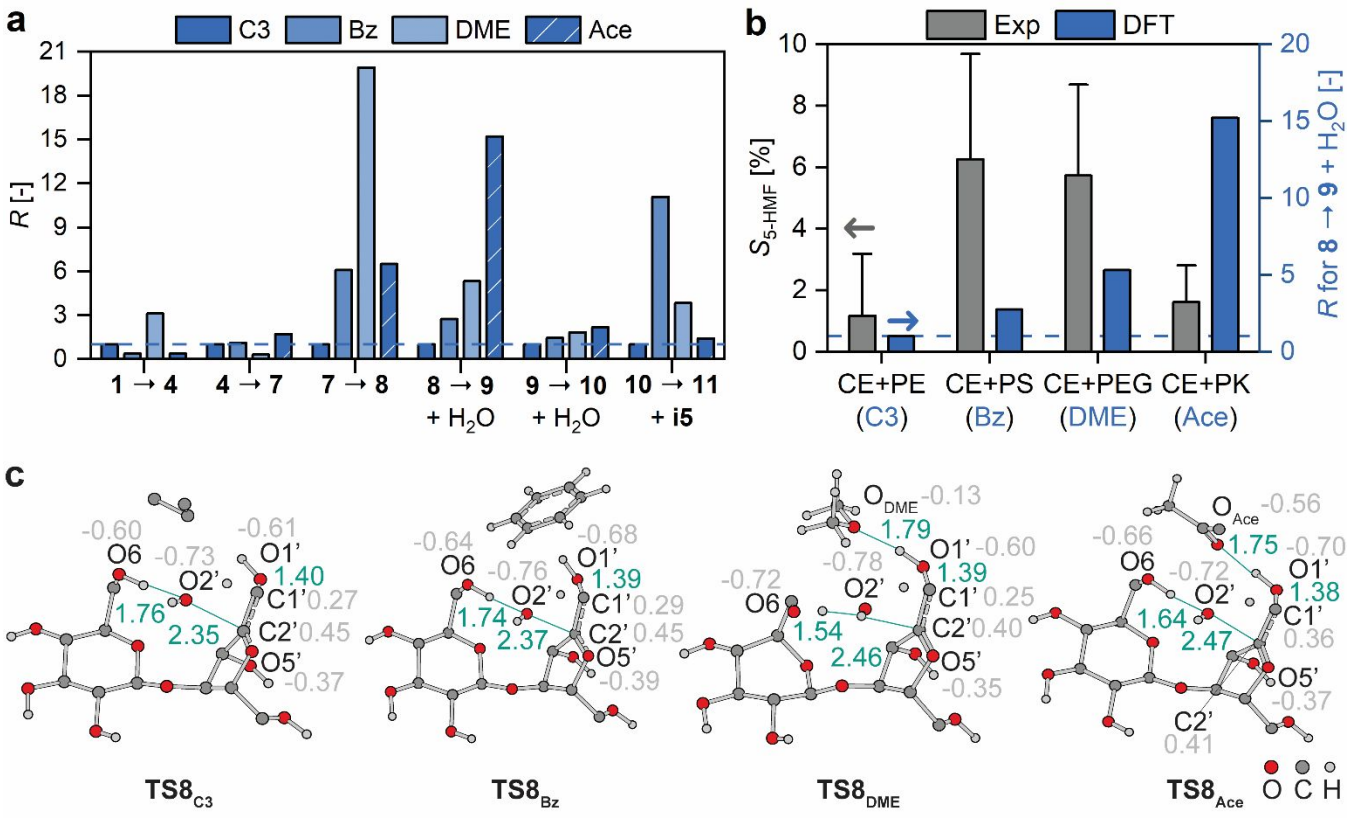

Figure 4. (a) DFT-calculated rate constant ratios (*R*) of the elementary steps of 5-hydroxymethylfurfural (5-HMF) formation in the presence of C3, Bz, DME, or Ace at 500°C. (b) Comparison of selectivity toward 5-HMF from the co-pyrolysis experiments of CE with PE (CE+PE), PS (CE+PS), PEG (CE+PEG), or PK (CE+PK) against the *R* values for the rate-limiting step **8** → **9** + H_2O in the presence of corresponding surrogates. (c) TSs for **8** → **9** + H_2O in the presence of C3, Bz, DME, or Ace including key distances and partial charges. Numbers in green and grey represent distances in Å and ChelpG partial charges in au, respectively. Hydrogen atoms not involved in noticeable interactions are omitted for clarity.

The DFT-calculated TSs for dehydration **8** → **9** + H_2O (**Figure 4c**) show that each functional group surrogate is forming an intermolecular hydrogen bond with the O1' hydroxyl group located near the reaction center. While Bz leads to O−H···π interaction with the O1' hydroxyl group, an O−H···O type hydrogen bond, stronger than the O−H···π type hydrogen bond, is formed between O1'−H and O_{DME} or O_{Ace}. This corresponds to the larger catalytic effect caused by the ether and ketone groups

than that caused by the aromatic groups. The O1'−H···O_{Ace} hydrogen bond of **TS8$_{Ace}$** is 0.04 Å shorter and thus stronger than O1'−H···O_{DME} of **TS8$_{DME}$**. The catalytic effect caused by each functional group is further evidenced by the increased distance between O2' and C2', where Ace leads to the largest increase by 0.12 Å, corresponding to the largest *R* value (**8** → **9** + H_2O, R_{Ace}=15.2).

Our DFT calculations reveal many possible NCIs induced by different plastic functional groups near the reaction centers of various CE pyrolysis pathways. The concert actions caused by the NCIs are shown to perturb TS bond lengths and partial charges and form intermolecular hydrogen bonds of different strengths, stabilizing or destabilizing the TSs to create catalytic and inhibitory effects.

Conclusion

The discovery of catalytic and inhibitory effects on cellulose fast pyrolysis caused by noncovalent interactions (NCIs) induced by the aromatic, ether, and ketone functional groups in molten plastics is reported. Molecular-level understanding of the NCI induced chemistry was studied by microreactor experiments and DFT. Our microreactor experiments demonstrated that the selectivity toward cellulose-derived anhydrosugars, small oxygenates, or furans each increased in the presence of polyketone, polyethylene glycol, or polystyrene. The change in experimental product distributions is explained by DFT calculations, revealing that NCIs induced by molten plastic functional groups perturb the geometries and partial charges of the transition states of key cellulose pyrolysis reactions, creating transition-state stabilization or destabilization and thus catalytic or inhibitory effects. In-depth understanding of transition-state perturbation presented in this work offers opportunities for further manipulation of NCIs[53] for tunable cellulose fast pyrolysis using new designs of molten plastics as unconventional catalysts or inhibitors.[54] Furthermore, the reported kinetic parameters could be incorporated into a microkinetic model to predict time evolution of product formation from cellulose fast pyrolysis in the presence of molten plastics, thereby advancing efficient design of biomass pyrolysis processes targeting specific bio-based chemicals.**Supporting Information**

Materials, methods, supporting experimental and computational data.

Conflict of interest

There are no conflicts to declare.

Acknowledgements

This work was supported by the National Science Foundation (Award Number CBET-1847289) and completed in part with resources provided by the University of Massachusetts' Green High Performance Computing Cluster (GHPCC).

ORCID

Hsi-Wu Wong: 0000-0003-2623-6145

Fuat Sakirler: 0000-0001-5144-0469

References

(1) Ragauskas, A. J.; Williams, C. K.; Davison, B. H.; Britovsek, G.; Cairney, J.; Eckert, C. A.; Frederick, W. J.; Hallett, J. P.; Leak, D. J.; Liotta, C. L.; et al. *Science* **2006**, *311*, 484-489.

(2) Mettler, M. S.; Vlachos, D. G.; Dauenhauer, P. J. *Energy Environ. Sci.* **2012**, *5*, 7797-7809.

(3) Liu, C.; Wang, H.; Karim, A. M.; Sun, J.; Wang, Y. *Chem. Soc. Rev.* **2014**, *43*, 7594-7623.

(4) Vispute, T. P.; Zhang, H.; Sanna, A.; Xiao, R.; Huber, G. W. *Science* **2010**, *330*, 1222-1227.

(5) Sharifzadeh, M.; Sadeqzadeh, M.; Guo, M.; Borhani, T. N.; Murthy Konda, N. V. S. N.; Garcia, M. C.; Wang, L.; Hallett, J.; Shah, N. *Prog. Energy Combust. Sci.* **2019**, *71*, 1-80.

(6) MacLeod, M.; Arp, H. P. H.; Tekman, M. B.; Jahnke, A. *Science* **2021**, *373*, 61-65.

(7) Rochman, C. M.; Browne, M. A.; Halpern, B. S.; Hentschel, B. T.; Hoh, E.; Karapanagioti, H. K.; Rios-Mendoza, L. M.; Takada, H.; Teh, S.; Thompson, R. C. *Nature* **2013**, *494*, 169-171.

(8) *Advancing Sustainable Materials Management: 2018 Tables and Figures*; United States Environmental Protection Agency, 2020. https://www.epa.gov/sites/default/files/2021-01/documents/2018_tables_and_figures_dec_2020_fnl_508.pdf.

(9) Garcia, J. M.; Robertson, M. L. *Science* **2017**, *358*, 870-872.

(10) Brooks, J. G.; Goforth, B. D.; Goforth, C. L. Recycling plastic coated paper product waste. US Patent 5,084,135, 1992.

(11) Brooks, J. G.; Goforth, B. D.; Goforth, C. L. Method for recycling plastic coated paper product waste and polymeric film. US Patent 5,277,758, 1994.

(12) Zhang, X.; Lei, H.; Zhu, L.; Zhu, X.; Qian, M.; Yadavalli, G.; Wu, J.; Chen, S. *Bioresour. Technol.* **2016**, *220*, 233-238.

(13) Ahmed, M. H. M.; Batalha, N.; Mahmudul, H. M. D.; Perkins, G.; Konarova, M. *Bioresour. Technol.* **2020**, *310*, 123457.

(14) Wang, Z.; Burra, K. G.; Lei, T.; Gupta, A. K. *Prog. Energy Combust. Sci.* **2021**, *84*, 100899.

(15) Vinu, R.; Broadbelt, L. J. *Energy Environ. Sci.* **2012**, *5*, 9808-9826.

(16) Westerhout, R. W. J.; Waanders, J.; Kuipers, J. A. M.; van Swaaij, W. P. M. *Ind. Eng. Chem. Res.* **1997**, *36*, 1955-1964.

(17) Westerhout, R. W. J.; Balk, R. H. P.; Meijer, R.; Kuipers, J. A. M.; van Swaaij, W. P. M. *Ind. Eng. Chem. Res.* **1997**, *36*, 3360-3368.

(18) Bhattacharya, P.; Steele, P. H.; Hassan, E. B. M.; Mitchell, B.; Ingram, L.; Jr., C. U. P. *Fuel* **2009**, *88*, 1251-1260.

(19) Dong, C.; Yang, Y.; Jin, B.; Horio, M. *Waste Manage.* **2007**, *27*, 1557-1561.

(20) Matsuzawa, Y.; Ayabe, M.; Nishino, J. *Polym. Degrad. Stab.* **2001**, *71*, 435-444.

(21) Dorado, C.; Mullen, C. A.; Boateng, A. A. *ACS Sustainable Chem. Eng.* **2014**, *2*, 301-311.

(22) Zhang, X.; Lei, H.; Chen, S.; Wu, J. *Green Chem.* **2016**, *18*, 4145-4169.

(23) Dorado, C.; Mullen, C. A.; Boateng, A. A. *Appl. Catal. B* **2015**, *162*, 338-345.

(24) Kasataka, K.; Kumagai, S.; Kameda, T.; Saito, Y.; Yoshioka, T. *Bioresour. Technol. Rep.* **2020**, *11*, 100431.

(25) Liu, X.; Burra, K. G.; Wang, Z.; Li, J.; Che, D.; Gupta, A. K. *Appl. Energy* **2020**, *279*, 115811.

(26) Părpăriţă, E.; Nistor, M. T.; Popescu, M.-C.; Vasile, C. *Polym. Degrad. Stab.* **2014**, *109*, 13-20.

(27) Kumagai, S.; Fujita, K.; Takahashi, Y.; Nakai, Y.; Kameda, T.; Saito, Y.; Yoshioka, T. *Sci. Rep.* **2019**, *9*, 1955.

(28) Nallar, M.; Wong, H.-W. *ACS Sustainable Chem. Eng.* **2019**, *7*, 9480-9488.

(29) Nallar, M.; Wong, H.-W. *Ind. Eng. Chem. Res.* **2019**, *58*, 10776-10784.

(30) Maduskar, S.; Maliekkal, V.; Neurock, M.; Dauenhauer, P. J. *ACS Sustainable Chem. Eng.* **2018**, *6*, 7017-7025.

(31) Sakirler, F.; Wong, H.-W. *J. Phys. Chem. A* **2022**, *126*, 7806-7819.

(32) Zhu, C.; Maduskar, S.; Paulsen, A. D.; Dauenhauer, P. J. *ChemCatChem* **2016**, *8*, 818-829.

(33) Pecha, M. B.; Montoya, J. I.; Chejne, F.; Garcia-Perez, M. *Ind. Eng. Chem. Res.* **2017**, *56*, 4288-4301.

(34) Westerhof, R. J. M.; Oudenhoven, S. R. G.; Marathe, P. S.; Engelen, M.; Garcia-Perez, M.; Wang, Z.; Kersten, S. R. A. *React. Chem. Eng.* **2016**, *1*, 555-566.

(35) Kumagai, S.; Fujita, K.; Takahashi, Y.; Kameda, T.; Saito, Y.; Yoshioka, T. *J. Jpn. Inst. Energy* **2019**, *98*, 202-219.

(36) Mayes, H. B.; Nolte, M. W.; Beckham, G. T.; Shanks, B. H.; Broadbelt, L. J. *ACS Sustainable Chem. Eng.* **2014**, *2*, 1461-1473.

(37) Lu, Q.; Hu, B.; Zhang, Z.-x.; Wu, Y.-t.; Cui, M.-s.; Liu, D.-j.; Dong, C.-q.; Yang, Y.-p. *Combust. Flame* **2018**, *198*, 267-277.

(38) Hu, B.; Zhang, B.; Xie, W.-l.; Jiang, X.-y.; Liu, J.; Lu, Q. *Energy Fuels* **2020**, *34*, 10384-10440.

(39) Lin, Y.-C.; Cho, J.; Tompsett, G. A.; Westmoreland, P. R.; Huber, G. W. *J. Phys. Chem. C* **2009**, *113*, 20097-20107.

(40) Mettler, M. S.; Paulsen, A. D.; Vlachos, D. G.; Dauenhauer, P. J. *Green Chem.* **2012**, *14*, 1284-1288.

(41) Seshadri, V.; Westmoreland, P. R. *J. Phys. Chem. A* **2012**, *116*, 11997-12013.

(42) Mayes, H. B.; Nolte, M. W.; Beckham, G. T.; Shanks, B. H.; Broadbelt, L. J. *ACS Catal.* **2015**, *5*, 192-202.

(43) Hosoya, T.; Sakaki, S. *ChemSusChem* **2013**, *6*, 2356-2368.

(44) Neel, A. J.; Hilton, M. J.; Sigman, M. S.; Toste, F. D. *Nature* **2017**, *543*, 637-646.

(45) Chen, L.; Zhao, J.; Pradhan, S.; Brinson, B. E.; Scuseria, G. E.; Zhang, Z. C.; Wong, M. S. *Green Chem.* **2016**, *18*, 5438-5447.

(46) Paine, J. B.; Pithawalla, Y. B.; Naworal, J. D. *J. Anal. Appl. Pyrol.* **2008**, *82*, 10-41.

(47) Zhou, X.; Mayes, H. B.; Broadbelt, L. J.; Nolte, M. W.; Shanks, B. H. *AIChE J.* **2016**, *62*, 766-777.

(48) Zhang, J.; Choi, Y. S.; Yoo, C. G.; Kim, T. H.; Brown, R. C.; Shanks, B. H. *ACS Sustainable Chem. Eng.* **2015**, *3*, 293-301.

(49) Nørskov, J. K.; Bligaard, T.; Kleis, J. *Science* **2009**, *324*, 1655-1656.

(50) Kozuch, S.; Martin, J. M. L. *ChemPhysChem* **2011**, *12*, 1413-1418.

(51) Campbell, C. T. *ACS Catal.* **2017**, *7*, 2770-2779.

(52) Zhou, X.; Mayes, H. B.; Broadbelt, L. J.; Nolte, M. W.; Shanks, B. H. *AIChE J.* **2016**, *62*, 778-791.

(53) Wheeler, S. E.; Seguin, T. J.; Guan, Y.; Doney, A. C. *Acc. Chem. Res.* **2016**, *49*, 1061-1069.

(54) Sigman, M. S.; Harper, K. C.; Bess, E. N.; Milo, A. *Acc. Chem. Res.* **2016**, *49*, 1292-1301.